Thermal response of a Maxwell fluid in oscillatory boundary layer flow over a wavy wall

J. Carlos Domínguez-Lozoya
Facultad de Ciencias Físico-Matemáticas, Universidad Autónoma de Sinaloa, Ciudad Universitaria, Culiacán, 80010, Sinaloa, México

S. Cuevas
Instituto de Energías Renovables, Universidad Nacional Autónoma de México, Temixco, 62580, Morelos, México

L. Córdova-Castillo
Centro de Ingeniería y Desarrollo Industrial, Pie de la Cuesta 702, 76125, Querétaro, México.

C. A. Martínez-Félix
Facultad de Ciencias Físico-Matemáticas, Universidad Autónoma de Sinaloa, Ciudad Universitaria, Culiacán, 80010, Sinaloa, México

Received 14 August 2025; accepted 15 January 2025

The thermal behavior of a viscoelastic fluid, modeled using the linear Maxwell model, is analyzed in oscillatory boundary layer flow over a wavy wall. Based on a previously derived velocity field (Cuevas *et al*. J. Non-Newton. Fluid Mech. 321 (2023) 105125) that assumes both a small oscillation amplitude and a Stokes layer thickness much smaller than the wall wavelength, the heat transfer equation is solved using a perturbation method. A time-harmonic temperature is prescribed at the wall, and a constant temperature is imposed at the outer edge of the boundary layer. The first order solution corresponds to the thermal analogue of the Stokes' second problem and is independent of the viscoelasticity of the fluid. At second order, convective heat transport gives rise to a temperature field composed of a time-periodic component and a steady distribution, analogous to the steady streaming observed in the corresponding flow problem. The non-vanishing steady temperature at the edge of the inner thermal layer leads to a generalized form of the Rayleigh's law of streaming for the thermal viscoelastic case and, consequently, to the formation of an outer thermal layer whose thickness is estimated.

Keywords: Oscillatory flow; wavy wall; thermal boundary layer; steady streaming; Maxwell viscoelastic fluid.

DOI: https://doi.org/10.31349/RevMexFis.72.020604

1. Introduction

Oscillatory flows are central to numerous technological applications-for instance, in enhancing heat [1,2] and mass transfer [3,4], and in energy conversion devices [5]-and also play a key role in natural phenomena within oceanographic [6,7] and physiological contexts [8,9]. The archetypical oscillatory flow, the Stokes' second problem [10], often emerges in the analysis of oscillatory boundary layer flows and commonly serves as a foundational reference for analyzing more intricate scenarios. While Stokes' solution is limited to linear viscous interactions of an oscillating fluid with a solid wall, convective terms introduce non-linear effects that may lead to the steady streaming phenomenon [11], namely, a sustained recirculating flow induced by a primary oscillatory motion of zero mean, typically generated by vibrating boundaries or periodic pressure fluctuations. This effect arises at second order within the framework of unsteady boundary layer theory [12], where the nonlinear Reynolds stresses give rise to a non-vanishing time-averaged flow in the near-wall region. A defining characteristic of steady streaming is its viscous penetration beyond the oscillatory boundary layer, leading to the establishment of a persistent mean flow in the outer region [13].

Rayleigh [14,15] provided the first theoretical explanation of streaming generated by acoustic waves. By employing a successive approximation method-where the solution to the linear problem serves as the forcing term in the second-order governing equations-this methodology has become the prevailing analytical framework for studying steady streaming. Another significant contribution was made by Schlichting [16,17], who applied boundary layer theory to match the solutions of the inner and outer layers in the problem of an oscillating cylinder. A classification framework based on the streaming Reynolds number, R_s, was established by Stuart [13], who showed that in the limit $R_s \gg 1$, a secondary boundary layer of thickness $\mathrm{O}(L/\sqrt{R_s})$ develops, within which the steady streaming velocity decays to zero, where L is the characteristic length of the flow. In turn, Riley made significant contributions by employing the method of matched asymptotic expansions to investigate the phenomenon [11,12,18,19].

In the past few decades steady streaming has aroused growing interest owing to innovative microfluidic applica-

tions that primarily employ acoustic techniques to generate streaming [20]. For example, streaming induced by acoustic waves has been proposed as an effective strategy for enhancing mixing in microchannels [21,22] or for the manipulation of suspended particles [23]. Streaming vortices generated by fluid oscillation around a fixed cylinder in a microchannel have been employed to trap and suspend cells without surface contact [24]. Similarly, streaming flows produced by microbubbles have been used to achieve particle sorting [25]. To explore how elasticity affects streaming, Bhosale *et al*. [26] studied oscillatory flow around a submerged soft cylinder. Their results revealed that soft structures generate more pronounced streaming at lower frequencies, leading them to introduce the concept of soft streaming, which they suggest may be exploited by biological organisms due to their natural softness.

Since many fluids in microfluidic and biological applications exhibit non-Newtonian behavior, the study of oscillatory flows-particularly steady streaming-in non-Newtonian fluids is of significant relevance. However, aside from a few early studies on steady streaming flows in viscoelastic fluids under classical conditions-such as oscillating cylinders [27,28] and spheres [29,30] in quiescent fluids-comprehensive investigations of this phenomenon in microfluidic systems remain lacking.

While the flow dynamics of oscillatory boundary layers and steady streaming have been extensively investigated, their heat transfer characteristics have received comparatively less attention. As an extension of dynamic studies, early investigations examined the effect of streaming induced by oscillatory flows around cylinders and spheres on heat transfer. For instance, Richardson [31] explored heat transfer around a circular cylinder immersed in a fluid subjected to acoustic streaming, focusing on the effects of the induced flow on thermal transport. Davidson [32] employed matched asymptotic analysis and numerical simulations to study the heat transfer from a vibrating heated cylinder in the regimes of low and high streaming Reynolds numbers. In turn, Gopinath and Mills [33] conducted a comprehensive study on heat transfer from a hot oscillating sphere immersed in a quiescent fluid. In addition, they examined steady heat transfer induced by streaming flow within a cylindrical duct, where a constant temperature gradient was maintained across the duct ends[34]. Cuevas and Ramos [35] analytically studied the dynamic and thermal behavior of oscillatory boundary layer flow of an incompressible, electrically conducting Newtonian fluid under a magnetic field. They found that electromagnetic effects confine the streaming motion within the Stokes layer, in contrast to the hydrodynamic case, where streaming extends beyond it [13]. Motivated by the thermoacoustic streaming phenomenon of interest for thermoacoustic refrigeration devices, in an experimental study Gopinath and Harder [36] developed correlations for heat transfer from a cylinder in a low-amplitude zero-mean oscillatory flow. In turn, Gopinath [37] treated the thermoacoustic streaming on a rigid sphere in a strong standing acoustic field finding that the interaction of first-order harmonic quantities within the boundary layer generates not only the well-known second-order time-averaged flow, but also a second-order time-averaged temperature distribution. More recently, the use of acoustic streaming to enhance heat transfer has attracted considerable attention [38-40]. This interest arises from the fact that the flow pattern modifications induced by acoustic streaming around a solid body can influence the heat exchange between the body and its surrounding medium, and even enhance heat transfer under suitable conditions. In fact, the possibility of using the streaming phenomenon for heat transfer enhancement in microchannels has been explored [41,42].

Based on a previous work where the oscillatory boundary layer flow of a Maxwell fluid over a wavy wall was analyzed [43], the present study aims to contribute to the understanding of the thermal behavior of oscillatory boundary layers incorporating the effects of viscoelasticity. The wavy wall is introduced as a simplified representation of wall roughness, given the importance of geometric perturbations at the microscale, as has been examined in various studies on microchannel flows of both Newtonian and non-Newtonian fluids [44-46]. Given that wall waviness plays a crucial role in the emergence of steady streaming, it has a direct impact on the thermal behavior of the boundary layer. Our analysis focuses particularly on how the thermal boundary layer characteristics are modified by the viscoelastic properties of the fluid, and how the steady streaming phenomenon, which was shown to be significantly affected by the fluid's elasticity [43], influences the heat transfer process. The results provide insights into the interplay between viscoelasticity, oscillatory flow, and thermal transport in boundary layer flows over curved surfaces and generalize a classical problem of current interest for microfluidic applications.

2. Formulation of the problem

We consider the heat transfer that takes place in the boundary layer oscillatory flow of an incompressible viscoelastic fluid

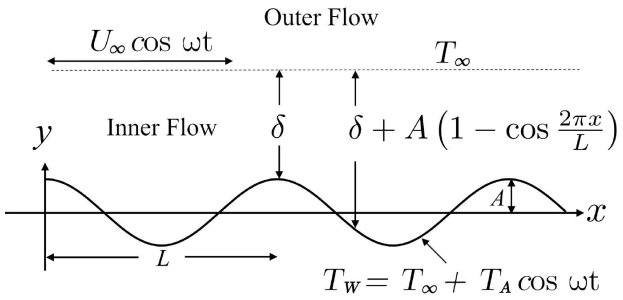

FIGURE 1. Sketch of the oscillatory boundary-layer flow over a wavy wall under non-isothermal conditions. A harmonic potential flow oscillates in the outer region above the wavy surface, generating a boundary-layer flow and associated heat transfer. δ is the boundary layer thickness, while A and L are the amplitude and wavelength of the wall.

limited by a motionless infinite wavy wall which is described by the equation $y_w = A\cos(2\pi x/L)$, where A and L are the amplitude and wavelength of the wall, while x is the streamwise coordinate. The flow is driven by a harmonic pressure gradient applied in the x-direction, in such a way that outside the boundary layer the fluid performs a unidirectional zero-mean oscillatory irrotational motion whose axial velocity can be expressed as $U_\infty \cos\omega t$, where U_∞ is the velocity amplitude and ω is the angular frequency of the oscillation. The temperature in the outer flow takes a uniform value, T_∞, while at the wavy wall the temperature undergoes a periodic oscillation that can be expressed as $T_w = T_\infty + T_A \cos\omega t$, where T_A is the amplitude of the oscillation. The configuration of the problem is schematically presented in Fig. 1.

The mass and momentum conservation equations along with the heat transfer equation can be expressed in the form

$$\nabla \cdot \mathbf{u} = 0, \tag{1}$$

$$\rho\left(\frac{\partial \mathbf{u}}{\partial t} + (\mathbf{u}\cdot\nabla)\mathbf{u}\right) = -\nabla p - \nabla\cdot\boldsymbol{\sigma}, \tag{2}$$

$$\rho C_p\left(\frac{\partial T}{\partial t} + (\mathbf{u}\cdot\nabla)T\right) = k\nabla^2 T, \tag{3}$$

where $\mathbf{u}$ is the velocity field, p is the pressure field, $\boldsymbol{\sigma}$ is the stress tensor, T is the temperature field, ρ is the mass density, C_p is the specific heat at constant pressure and k is the thermal conductivity. Natural convection and viscous dissipation are disregarded in the present study.

The viscoelastic character of the fluid is introduced through the upper convected Maxwell model whose constitutive equation in the linear approximation is expressed as [43,47,48]

$$t_m\frac{\partial \boldsymbol{\sigma}}{\partial t} = -\mu[\nabla\mathbf{u} + (\nabla\mathbf{u})^T] - \boldsymbol{\sigma}, \tag{4}$$

where t_m is the Maxwell relaxation time and μ is the dynamic viscosity. Note that when $t_m = 0$, the constitutive equation for a Newtonian fluid is recovered.

It can be shown [43] that conservation Eqs. (1)-(3) can be combined with Eq. (4) so that, for a two-dimensional flow, governing equations can be expressed as

$$\frac{\partial u}{\partial x} + \frac{\partial v}{\partial y} = 0, \tag{5}$$

$$\left(1 + t_m\frac{\partial}{\partial t}\right)\left[\frac{\partial u}{\partial t} + u\frac{\partial u}{\partial x} + v\frac{\partial u}{\partial y}\right] = -\frac{1}{\rho}\left(1 + t_m\frac{\partial}{\partial t}\right)\frac{\partial p}{\partial x} + \frac{\mu}{\rho}\left(\frac{\partial^2 u}{\partial x^2} + \frac{\partial^2 u}{\partial y^2}\right), \tag{6}$$

$$\left(1 + t_m\frac{\partial}{\partial t}\right)\left[\frac{\partial v}{\partial t} + u\frac{\partial v}{\partial x} + v\frac{\partial v}{\partial y}\right] = -\frac{1}{\rho}\left(1 + t_m\frac{\partial}{\partial t}\right)\frac{\partial p}{\partial y} + \frac{\mu}{\rho}\left(\frac{\partial^2 v}{\partial x^2} + \frac{\partial^2 v}{\partial y^2}\right), \tag{7}$$

$$\frac{\partial T}{\partial t} + u\frac{\partial T}{\partial x} + v\frac{\partial T}{\partial y} = \frac{k}{\rho C_p}\left(\frac{\partial^2 T}{\partial x^2} + \frac{\partial^2 T}{\partial y^2}\right), \tag{8}$$

where u and v are the velocity components in the streamwise and transverse directions, respectively. We now introduce the following non-dimensional variables

$$\tau = t\omega, \quad X = \frac{x}{L}, \quad Y = \frac{y}{\delta}, \quad \overline{u} = \frac{u}{U_\infty}, \quad \overline{p} = \frac{2p}{\rho\omega U_\infty L}, \quad \overline{v} = \frac{Lv}{\delta U_\infty}, \quad \Theta = \frac{T - T_\infty}{T_A}, \tag{9}$$

where δ is the Stokes layer thickness, $\delta = \sqrt{2\nu/\omega}$, being $\nu = \mu/\rho$ the kinematic viscosity. We assume that the wavelength of the wavy wall significantly exceeds the thickness of the Stokes layer, that is, $L \gg \delta$. As it is shown in Ref. [43], under this approximation axial viscous diffusion terms as well as the transverse pressure gradient can be neglected, therefore, governing equations in dimensionless form reduce to a boundary layer problem

$$\frac{\partial u}{\partial X} + \frac{\partial v}{\partial Y} = 0, \tag{10}$$

$$\left(1 + De\frac{\partial}{\partial \tau}\right)\left[2\frac{\partial u}{\partial \tau} + 2\varepsilon\left(u\frac{\partial u}{\partial X} + v\frac{\partial u}{\partial Y}\right)\right] = -\left(1 + De\frac{\partial}{\partial \tau}\right)\frac{\partial p}{\partial X} + \frac{\partial^2 u}{\partial Y^2}, \tag{11}$$

$$2Pr\frac{\partial \Theta}{\partial \tau} + 2Pr\varepsilon\left[u\frac{\partial \Theta}{\partial X} + v\frac{\partial \Theta}{\partial Y}\right] = \frac{\partial^2 \Theta}{\partial Y^2}, \tag{12}$$

which must satisfy the non-slip condition and the oscillating temperature at the wavy wall and the matching of the streamwise velocity and temperature outside the boundary layer, namely,

$$u = v = 0 \quad \text{at} \quad Y = Y_w = a\cos(2\pi X), \tag{13}$$

$$u = \cos\tau \quad \text{as} \quad Y \to \infty, \tag{14}$$

$$\Theta = \cos\tau \quad \text{at} \quad Y = Y_w = a\cos(2\pi X), \tag{15}$$

$$\Theta = 0; \quad \text{as} \quad Y \to \infty, \tag{16}$$

where $a = A/\delta$ is the dimensionless amplitude of the wall. Equations (11) and (12) involve relevant dimensionless parameters, $\varepsilon = U_\infty/\omega L$, $De = \omega t_m$ and $Pr = \nu/\alpha_T$, where α_T is the thermal diffusivity. The parameter ε can be interpreted as the ratio of the displacement amplitude of the fluid, U_∞/ω, to the wavelength of the wall, L. To ensure the absence of boundary layer separation, we will assume that the small amplitude of oscillation condition holds, that is, $\varepsilon \ll 1$ [13]. De is known as the Deborah number and is the ratio of the Maxwell relaxation time, t_m, and the characteristic time of the imposed oscillation, $1/\omega$. Moreover, Pr is the Prandtl number which is the ratio of the viscous and thermal diffusivities.

In order to simplify the mathematical treatment, it is convenient to adopt a reference frame in which the wall appears flat. This is accomplished by applying the following coordinate transformation: $\chi = X$ and $\eta = Y - Y_w$. According to this transformation and the incompressibility condition, it can be shown [43] that the dimensionless outer flow can be expressed as

$$U(\chi,\tau) = \Re\left\{U_o(\chi)\, e^{i\tau}\right\}, \tag{17}$$

where $\Re\{\}$ represents the real part of the quantity inside the brackets, while

$$U_o(\chi) = \left[1 + a(1 - \cos(2\pi\chi))\right]^{-1}. \tag{18}$$

The outer irrotational flow must, in turn, satisfy the momentum balance equation:

$$\left(1 + De\frac{\partial}{\partial\tau}\right)\left[2\frac{\partial U}{\partial\tau} + 2\varepsilon U\frac{\partial U}{\partial\chi}\right] = -\left(1 + De\frac{\partial}{\partial\tau}\right)\frac{\partial p}{\partial\chi}, \tag{19}$$

which expresses the pressure gradient established to counterbalance the inertia outside the boundary layer. In fact, within the framework of boundary-layer theory, the pressure distribution inside and outside the boundary layer is the same. For completeness, the pressure field is presented in Appendix A. Taking into account the coordinate transformation and using (19) to eliminate the axial pressure gradient, Eqs. (10), (11) and (12) become

$$\frac{\partial u}{\partial\chi} + 2a\pi\sin(2\pi\chi)\frac{\partial u}{\partial\eta} + \frac{\partial v}{\partial\eta} = 0, \tag{20}$$

$$\left(1 + De\frac{\partial}{\partial\tau}\right)\left(2\frac{\partial u}{\partial\tau} - 2\frac{\partial U}{\partial\tau}\right) - \frac{\partial^2 u}{\partial\eta^2} = 2\varepsilon\left(1 + De\frac{\partial}{\partial\tau}\right)\left[U\frac{\partial U}{\partial\chi} - u\left(\frac{\partial u}{\partial\chi} + 2a\pi\sin(2\pi\chi)\frac{\partial u}{\partial\eta}\right) - v\frac{\partial u}{\partial\eta}\right], \tag{21}$$

$$2\frac{\partial\Theta}{\partial\tau} - \frac{1}{Pr}\frac{\partial^2\Theta}{\partial\eta^2} = -2\varepsilon\Big[u\left(\frac{\partial\Theta}{\partial\chi} + 2a\pi\sin(2\pi\chi)\frac{\partial\Theta}{\partial\eta}\right) + v\frac{\partial\Theta}{\partial\eta}\Big], \tag{22}$$

while

$$u = v = 0 \quad \text{at} \quad \eta = 0, \tag{23}$$

$$u \to U(\chi,\tau) \quad \text{as} \quad \eta \to \infty, \tag{24}$$

$$\Theta = R\{e^{i\tau}\} \quad \text{at} \quad \eta = 0, \tag{25}$$

$$\Theta \to 0 \quad \text{as} \quad \eta \to \infty, \tag{26}$$

are the boundary conditions that must be satisfied.

3. Perturbation solution

We now look for solutions for the streamwise and the transversal velocity components, u and v, and the temperature, Θ, as perturbation expansions on the small parameter ε for arbitrary values of De, Pr and a, that is,

$$u(\chi,\eta,\tau) = u_0(\chi,\eta,\tau) + \varepsilon u_1(\chi,\eta,\tau) + \mathcal{O}(\varepsilon^2), \tag{27}$$

$$v(\chi,\eta,\tau) = v_0(\chi,\eta,\tau) + \varepsilon v_1(\chi,\eta,\tau) + \mathcal{O}(\varepsilon^2), \tag{28}$$

$$\Theta(\chi,\eta,\tau) = \Theta_0(\chi,\eta,\tau) + \varepsilon \Theta_1(\chi,\eta,\tau) + \mathcal{O}(\varepsilon^2), \tag{29}$$

where subscripts 0 and 1 denote the first and second order approximations, respectively. The solution of Eqs. (20) and (21), under the corresponding boundary conditions, were obtained in Ref. [43]. It was found that the relative motion between the fluid and the motionless wavy wall serves as a source of vorticity, giving rise to a primary oscillatory flow at order $\mathcal{O}(\varepsilon^0)$, and a order $\mathcal{O}(\varepsilon^1)$ secondary flow due to nonlinear effects. At order $\mathcal{O}(\varepsilon^0)$, the problem reduces to the generalized Stokes' second problem for a Maxwell fluid, where the solution for the streamwise velocity component exhibits an underdamped behavior. At order $\mathcal{O}(\varepsilon^1)$, the flow consists of a superposition of a periodic component with twice the original frequency and a steady part, commonly referred to as steady streaming arising from nonlinear Reynolds stresses.

In what follows, we will concentrate on solving the thermal behavior of the flow reported in Ref. [43].

3.1. First-order approximation

By substituting expansions (27), (28) and (29) in (22) and equating coefficients of powers of ε, at $\mathcal{O}(\varepsilon^0)$ we obtain

$$2\frac{\partial \Theta_0}{\partial \tau} - \frac{1}{Pr}\frac{\partial^2 \Theta_0}{\partial \eta^2} = 0, \tag{30}$$

with boundary conditions $\Theta_0(0,\tau) = e^{i\tau}$ and $\Theta(\infty,\tau) = 0$, which corresponds to a heat diffusion problem into a stagnant fluid. Note that it corresponds precisely to the thermal equivalent of the Stokes' second problem, whose solution is

$$\Theta_0(\eta,\tau) = \Re\{\kappa(\eta)e^{i\tau}\} = \Re\{e^{-\sqrt{Pr}(1+i)\eta}e^{i\tau}\}, \tag{31}$$

or explicitly

$$\Theta_0(\eta,\tau) = e^{-\sqrt{Pr}\eta}\cos\Big(\tau - \sqrt{Pr}\,\eta\Big). \tag{32}$$

As expected, the temperature inside the fluid is out of phase with respect to the temperature on the wall, the delay being modulated by the square root of the Prandtl number. When $Pr \to 0$ (perfect thermal conductor), the temperature of the fluid and the wall are in phase. Figure 2 shows the temperature distribution as a function of the transverse coordinate η at different times and a fixed Prandtl number, displaying the well-known dephasing of the Stokes' problem. The thermal penetration depth, δ_T, and the wavelength of the temperature distribution, λ_T, can be expressed as

$$\delta_T = \frac{\delta}{\sqrt{Pr}} = \sqrt{\frac{2\alpha_T}{\omega}}, \tag{33}$$

$$\lambda_T = \frac{\lambda_v}{\sqrt{Pr}} = 2\pi\sqrt{\frac{2\alpha_T}{\omega}} = 2\pi\frac{\delta}{\sqrt{Pr}}, \tag{34}$$

where $\lambda_v = 2\pi\delta$ is the wavelength for the viscous Stokes' second problem. We can observe that δ_T and λ_T coincide with their viscous counterparts when $Pr = 1$. Figure 3 shows the temperature distribution as a function of η for different Prandtl values at a given time, where it can be observed that the thermal penetration depth decreases as the Prandtl number increases. At this order, the solution is independent of the viscoelastic properties of the fluid.

3.2. Second-order approximation

At $\mathcal{O}(\varepsilon^1)$, the temperature distribution satisfies the equation

$$2\frac{\partial \Theta_1}{\partial \tau} - \frac{1}{Pr}\frac{\partial^2 \Theta_1}{\partial \eta^2} = -2\left[u_0\left(\frac{\partial \Theta_0}{\partial \chi} + 2a\pi\sin(2\pi\chi)\frac{\partial \Theta_0}{\partial \eta}\right) + v_0\frac{\partial \Theta_0}{\partial \eta}\right] \tag{35}$$

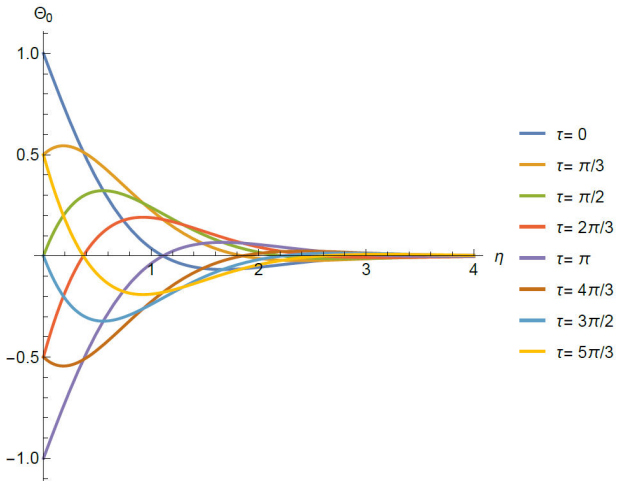

FIGURE 2. Temperature profile at $\mathcal{O}(\varepsilon^0)$ as a function of the transversal coordinate for different times with $Pr = 2$.

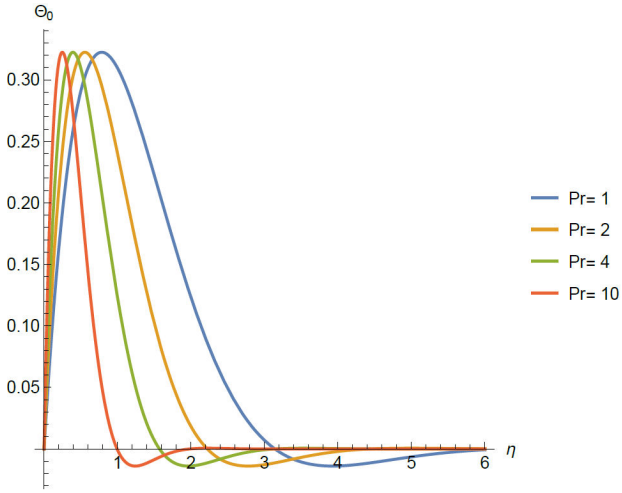

FIGURE 3. Temperature profile at $\mathcal{O}(\varepsilon^0)$ as a function of the transversal coordinate for different Prandtl numbers. $\tau = \pi/2$.

where the streamwise and transversal velocity components at order $\mathcal{O}(\varepsilon^0)$, u_0 and v_0, are expressed as [43]

$$u_0(\chi,\eta,\tau) = \Re\{U_0(\chi)\xi_0^{'}(\eta)e^{i\tau}\}, \tag{36}$$

$$v_0(\chi,\eta,\tau) = \Re\left\{\left[-\frac{dU_0}{d\chi}\xi_0(\eta) - 2\pi a U_0 \sin(2\pi\chi)\xi_0'(\eta)\right]e^{i\tau}\right\}, \tag{37}$$

where $\xi_0(\eta)$ has the form

$$\xi_0(\eta) = \eta - \frac{1}{\alpha+i\beta}\left(1 - e^{-(\alpha+i\beta)\eta}\right), \tag{38}$$

where

$$\alpha = \sqrt{\sqrt{1+De^2} - De}, \quad \beta = \sqrt{\sqrt{1+De^2} + De}.$$

Note that the right-hand side of (35) includes convective terms proportional to $\cos^2\tau = (1+\cos 2\tau)/2$. Hence, in addition to periodic terms of twice the original frequency, the convective contribution introduces time-independent terms that lead to a steady temperature field. Therefore, Θ_1 can be expressed in the form

$$\Theta_1(\chi,\eta,\tau) = \Re\left\{\frac{dU_0(\chi)}{d\chi}(\Upsilon_{1s}(\eta) + \Upsilon_{1u}(\eta)e^{2i\tau})\right\}, \tag{39}$$

where the subscripts u and s refer to the unsteady and steady parts, respectively. The equation that satisfies the unsteady contribution of Eq. (39) can be found by substituting (36)-(39) into (35), that is,

$$-\frac{1}{Pr}\frac{d^2\Upsilon_{1u}}{d\eta} + 4i\Upsilon_{1u} = -\lambda_0\xi_0(\eta)e^{-\lambda_0\eta}, \tag{40}$$

with boundary conditions

$$\Upsilon_{1u} = 0 \quad \eta = 0, \quad \text{and} \quad \Upsilon = 0 \quad \eta \to \infty, \tag{41}$$

where $\lambda_0 = \sqrt{Pr}(1+i)$.

The solution of equation (40) with the corresponding boundary conditions is given by

$$\begin{aligned}\Upsilon_{1u}(\eta) = {} & \frac{\lambda_0\lambda^2 e^{-\eta(2\lambda_0+2\lambda_2+\lambda_3)}}{\lambda_2(\lambda_0-\lambda_3)^2(\lambda_0+\lambda_3)^2(\lambda_0+\lambda_2-\lambda_3)(\lambda_0+\lambda_2+\lambda_3)}\Big[\lambda_2^2\big(-e^{2\eta(\lambda_0+\lambda_2)}\big)\big(3\lambda_0^2+2\lambda_0\lambda_2+\lambda_3^2\big) \\ & + (\lambda_0^2+2\lambda_0\lambda_2+\lambda_2^2-\lambda_3^2)e^{\eta(\lambda_0+2\lambda_2+\lambda_3)}\big(\lambda_0^2(\eta\lambda_2-1) \\ & + \lambda_3^2(1-\eta\lambda_2)+2\lambda_0\lambda_2\big) + (\lambda_0^2-\lambda_3^2)^2 e^{\eta(\lambda_0+\lambda_2+\lambda_3)}\Big]\end{aligned} \tag{42}$$

where $\lambda_0 = \lambda(1+i),\ \lambda_2 = \alpha + i\beta,\ \lambda_3 = \sqrt{4\lambda^2 i},\ \lambda = \sqrt{Pr}$.

On the other hand, the boundary value problem satisfied by the steady part, Υ_{1s}, is

$$-\frac{1}{Pr}\frac{\partial^2 \Upsilon_{1s}}{\partial \eta^2} = \frac{1}{2}\left(\xi_0 \overline{\frac{\partial \kappa}{\partial \eta}} + \overline{\xi_0}\frac{\partial \kappa}{\partial \eta}\right), \tag{43}$$

with boundary conditions $\Upsilon_{1s}(0) = 0$ and $\Upsilon_{1s}(\infty) = 0$. The overbar in Eq. (43) represents the conjugate complex quantities. As occurs in the fluid dynamic case, it is impossible to satisfy the condition $\Upsilon_{1s} \to 0$ as $\eta \to \infty$, if the condition $\Upsilon_{1s}(0) = 0$ is imposed at the wall. Therefore, the condition on Υ_{1s} at infinity must be relaxed by enforcing $\Upsilon_{1s}(\eta)$ to take a finite value as $\eta \longrightarrow \infty$. The solution of (43) that satisfies the relaxed boundary conditions is

$$\begin{aligned}\Upsilon_{1s} = \Big[&\lambda(\alpha+\beta)(\alpha^2+\beta^2)(\alpha^2+4\alpha\lambda+\beta^2-4\beta\lambda+6\lambda^2) + e^{-\eta(\alpha+\lambda)}(2\lambda^3(\alpha+\beta)(\alpha^2+4\alpha(\lambda-\beta)+\beta^2 \\ &- 4\beta\lambda+2\lambda^2)\cos(\eta(\lambda-\beta)) + e^{\alpha\eta}(\alpha^2+2\alpha\lambda+\beta^2+2\lambda(\lambda-\beta))^2(\lambda(\alpha^2\eta-\alpha+\beta(\beta\eta-1))\cos(\eta\lambda) \\ &- \sin(\eta\lambda)(\alpha^2(\eta\lambda+2)-\alpha\lambda+\beta(\beta\eta\lambda+2\beta+\lambda))) + 2\lambda^3(\alpha^3+3\alpha^2\beta-3\alpha\beta^2+2\lambda^2(\beta-\alpha) \\ &+ 8\alpha\beta\lambda-\beta^3)\sin(\eta(\lambda-\beta)))\Big] \Big/ \Big[2(\alpha^2+\beta^2)(\alpha^2+2\alpha\lambda+\beta^2+2\lambda(\lambda-\beta))^2\Big].\end{aligned} \tag{44}$$

Taking the limit when $De \to 0$ (negligible viscoelastic effects), (44) reduces to the corresponding expression for a Newtonian fluid:

$$\begin{aligned}\lim_{De\to 0}\Upsilon_{1s} = \Big(&\lambda + 3\lambda^3 + e^{-\eta(\lambda+1)}\Big[2\lambda^4\sin(\eta(\lambda-1)) + \left(\lambda^2-1\right)\lambda^3\cos(\eta(\lambda-1)) \\ &+ e^{\eta}\left(\lambda^2+1\right)^2\left[(\eta-1)\lambda\cos(\eta\lambda) - (\eta\lambda+2)\sin(\eta\lambda)\right]\Big]\Big)\left(\frac{1}{2\left(\lambda^2+1\right)^2}\right),\end{aligned} \tag{45}$$

which depends only on the Prandtl number. Solutions (44) and (45) correspond to the thermal equivalent of the well known steady streaming that appears in oscillatory flows as a result of nonlinear Reynolds stresses. In this case, the convective terms are responsible for the appearance of the steady thermal distribution. In fact, the second-order steady temperature field can be expressed as

$$\Theta_s = \varepsilon\Theta_{1s}(\eta,\chi) = \varepsilon\frac{dU_0}{d\chi}\Upsilon_{1s}(\eta). \tag{46}$$

Figure 4 shows the temperature fields (with superposed isotherms) within a wavelength of the wavy wall, obtained from (44) and (46) for a fixed Prandtl number ($Pr = 5$) and different values of the Deborah number, assuming that both the dimensionless wall amplitude, a, and the parameter ε are small ($a = 0.01$ and $\varepsilon = 0.01$). For $De = 0$, 5 and 10, vertically antisymmetric patterns are observed with a pair of elongated negative and positive temperature regions. As the Deborah number increases ($De > 10$), regions with inverted temperature close to the wall appear below the two elongated temperature regions. Isotherms of the steady temperature field present some similarity with the streamlines corresponding to the steady streaming flow [43]. The effect of the Prandtl number on the steady temperature is shown in Fig. 5 for a fixed Deborah number ($De = 10$). For low Prandtl numbers ($Pr \lesssim 1$) the regions with inverted temperature near the wall with closed isotherms show a substantial size which is reduced as the Prandtl number increases, and eventually disappears for $Pr \gtrsim 5$.

3.3. Thermal Rayleigh's law of streaming

Figure 6 shows the behavior of Υ_{1s} as a function of the transverse coordinate η for different Prandtl and Deborah numbers. It is found that for low Pr, negative values appear near the wavy wall. Using a Taylor series expansion of Υ_{1s} around $\eta = 0$, it is found that negative values arise when $Pr < (De^2+1)(-De+\sqrt{De^2+1})$, exhibiting a non-monotonic behavior. For the case when $De = 0$ (Newtonian case) negative values of Υ_{1s} appear when $Pr < 1$.

The most salient feature of the steady function Υ_{1s} observed in Fig. 6 is that for all cases, as η grows, it tends to a constant value that depends on Pr and De. Analogous to the behavior of the second-order tangential velocity component in the dynamical problem-which approaches a constant value rather than vanishing at the boundary layer edge, as described by Rayleigh's law of streaming [43] -a *thermal Rayleigh's law of streaming* can be formulated for a Maxwell fluid in the heat transfer problem as follows

$$\Theta_s = \varepsilon\frac{dU_0}{d\chi}F(De,Pr), \tag{47}$$

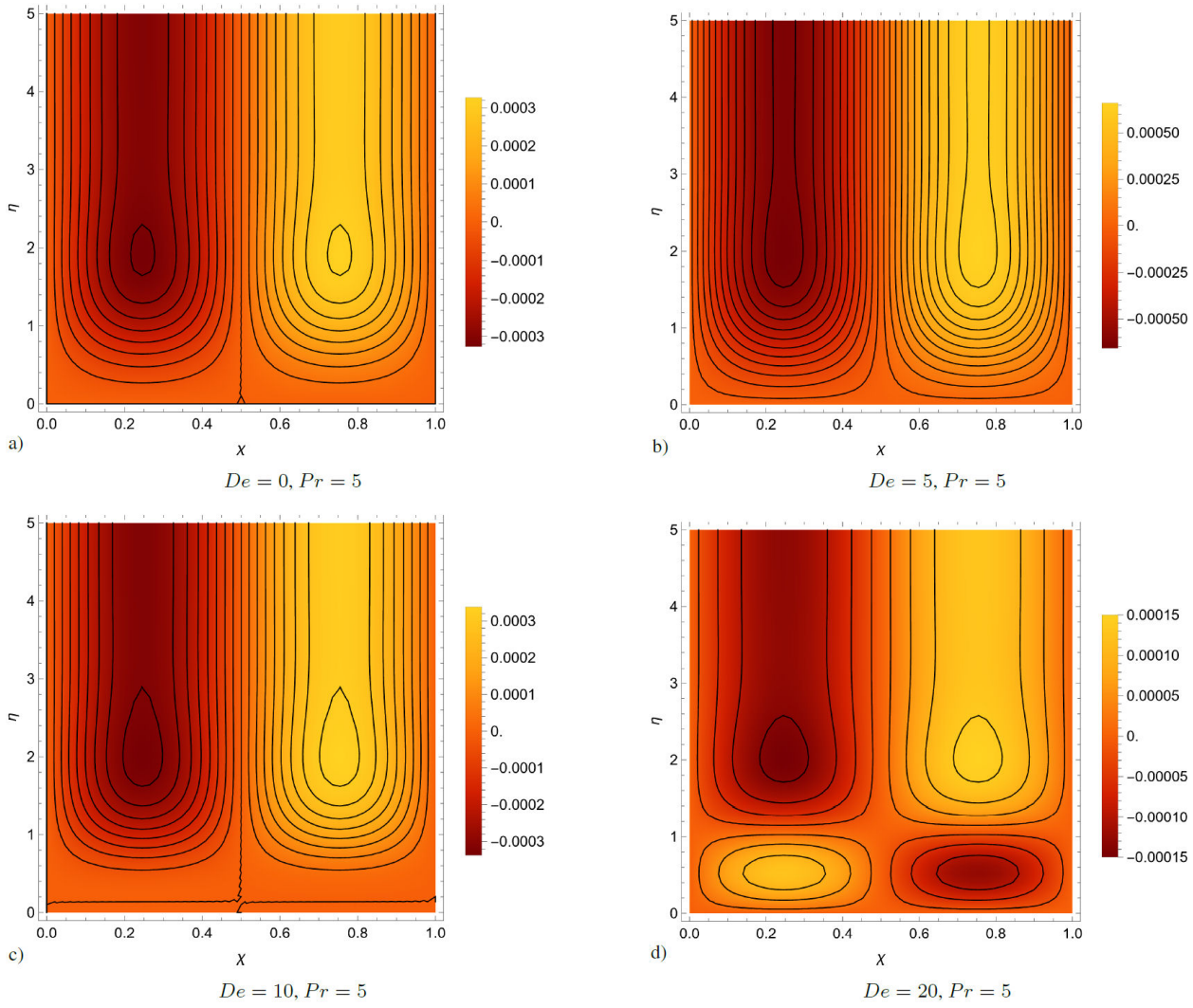

FIGURE 4. Steady temperature distribution within a wavelength for $\varepsilon = 0.01$, $a = 0.01$, $P_r = 5$ and different Deborah numbers.

where

$$F(De, Pr) = \lim_{\eta \to \infty} \Upsilon_{1s}(\eta) = \frac{\lambda(\alpha+\beta)\left(\alpha^2+\beta^2+4\alpha\lambda-4\beta\lambda+6\lambda^2\right)}{2\left(\alpha^2+\beta^2+2\alpha\lambda+2\lambda(\lambda-\beta)\right)^2}. \tag{48}$$

In the Newtonian limit $De \to 0$, Eq. (48) becomes $F(Pr) = (1+3Pr)/2Pr(1+Pr)^2$. The nonzero value of the temperature field at the edge of the boundary layer indicates the penetration of the steady temperature into the outer potential temperature field. This confirms the existence of an outer thermal region where the steady temperature decays to zero. Equations (47) and (48) show that the value of the temperature at the edge of the boundary layer depends, through Pr and De, on the diffusive and viscoelastic properties of the fluid. In fact, through asymptotic analysis, it is found that its maximum value is reached for the conditions $Pr = 1 + (2/\sqrt{3})$, in the Newtonian limit ($De = 0$), and $Pr = (1/6)(1+2De)$ when $De \gg 1$.

3.4. Estimation of the thickness of the outer thermal layer

In his classical paper, Stuart [13] identified the importance of the parameter $R_s = U_\infty^2/\omega\nu$, now named the streaming Reynolds number, for determining how the steady streaming velocity at the edge of the boundary layer decays to zero with distance from the wall. For small values of R_s, the outer flow is dominated by diffusion and governed by the linear Stokes equations. In contrast, for large values of R_s a secondary boundary layer (the outer layer) is formed, within which the steady flow driven by

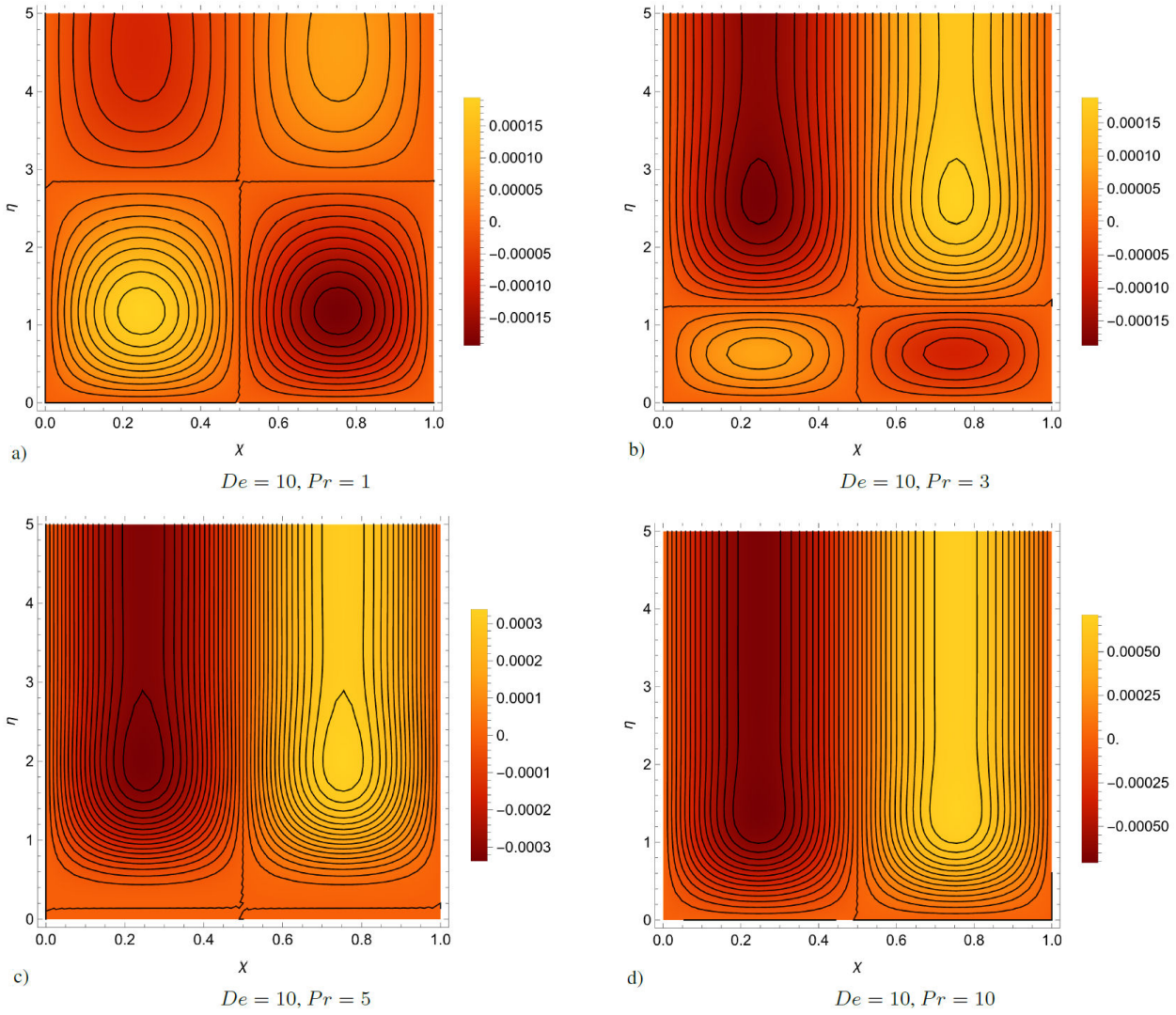

FIGURE 5. Steady temperature distribution within a wavelength for $\varepsilon = 0.01$, $a = 0.01$, $De = 10$ and different Prandtl number.

the non-zero velocity at the edge of the inner layer (*i.e.*, the Rayleigh's law of streaming), tends to zero. The generalization of this parameter for the flow of a Maxwell fluid is presented in Eq. [43].

Analogous to the steady streaming flow, we can define a *streaming Péclet number*, namely,

$$Pe_s = R_s Pr = \frac{U_\infty}{\omega \alpha_T} F(De, Pr) \tag{49}$$

which determines how the steady temperature at the edge of the inner thermal boundary layer decays to zero as the distance from the wall increases. For small values of Pe_s, a diffusion dominated heat transfer is established. In turn, for large values of Pe_s a secondary thermal boundary layer (the outer thermal layer) is formed. To match the internal temperature distribution with the external one, the relaxed finite temperature value (47) at the edge of the internal thermal boundary layer must be used as a boundary condition for the temperature distribution in the outer boundary layer. Since the main transition in the steady temperature pattern occurs for small values of the ratio Pr/De (*i.e.* $Pr/De < 0.5$, see Fig. 5), the limiting Θ_s value can be approximated for $Pr \ll 1$. Hence, by expanding $F(De, Pr)$ through a Taylor series, the thermal Rayleigh's law of streaming (47) reduces to

$$\Theta_s = \varepsilon \frac{dU_0}{d\chi} \left(\frac{\sqrt{\sqrt{\mathrm{De}^2+1} - \mathrm{De}} + \sqrt{\sqrt{\mathrm{De}^2+1} + \mathrm{De}}}{4\sqrt{\mathrm{De}^2+1}} \sqrt{\mathrm{Pr}} \right). \tag{50}$$

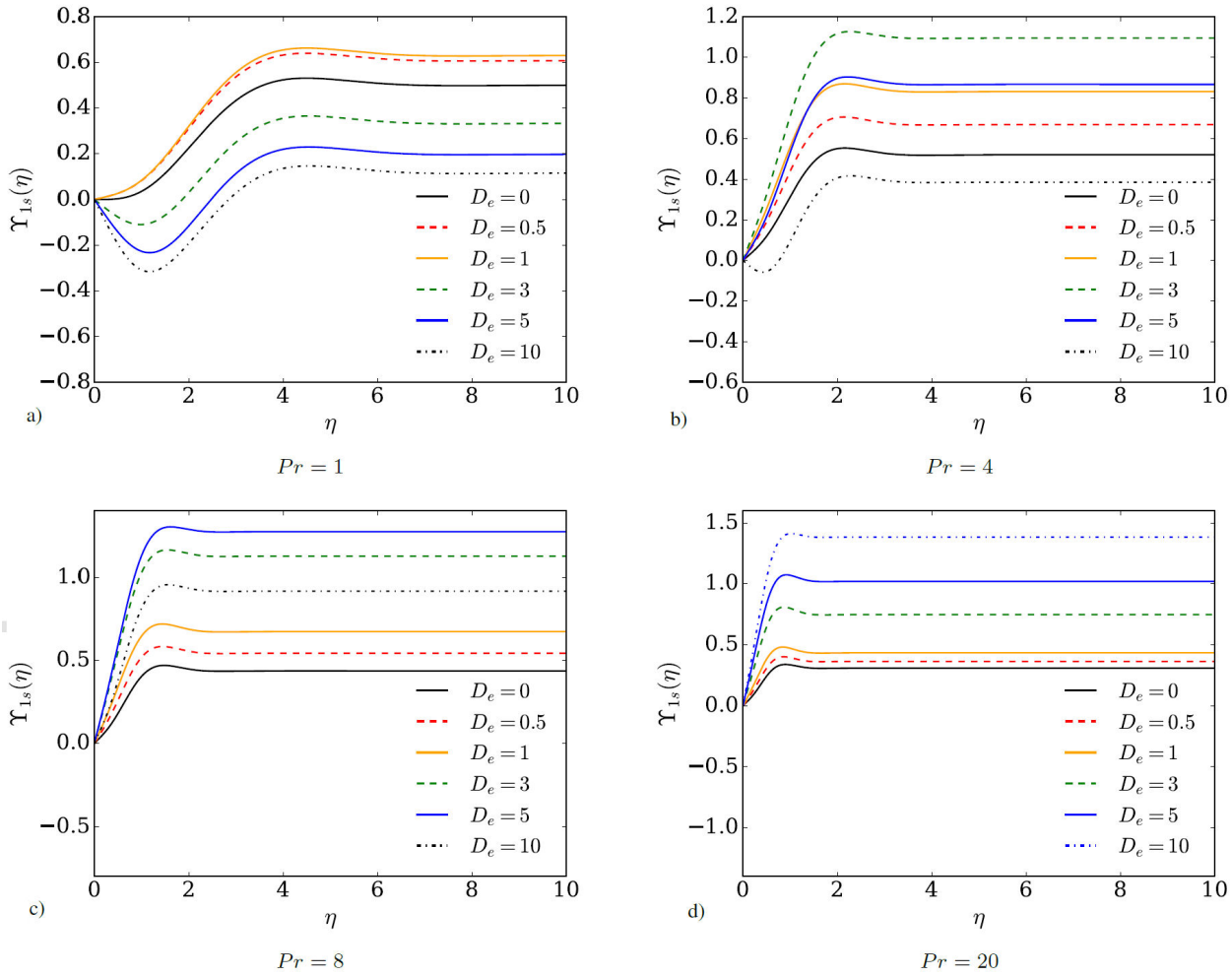

FIGURE 6. Υ_{1s} is plotted as a function of η for $P_r = 1$, 4, 8 and 20 and different Deborah numbers.

Finally, the thickness of the outer thermal boundary layer can be estimated from the balance between the diffusive term and the convective contribution responsible for the steady temperature in the heat transfer equation, namely,

$$\delta s_T = \varepsilon^{-1}\delta_T = \varepsilon^{-1}\frac{\delta}{\sqrt{Pr}}. \tag{51}$$

which is independent of the viscoelastic properties of the fluid.

3.5. Heat transfer

If we calculate the Nusselt number averaged over a wavelength of the wavy wall and one temporal cycle, we obtain

$$\langle \overline{Nu} \rangle = \int_0^{2\pi} \left[\int_0^1 -\frac{\partial \Theta}{\partial \eta}\bigg|_{\eta=0} d\chi \right] d\tau = 0, \tag{52}$$

which means that the net heat flux from the wall to the fluid is zero. This behavior arises from the periodic nature of the temperature field in time and along the axial direction. Result (52), however, may be misleading because the contribution

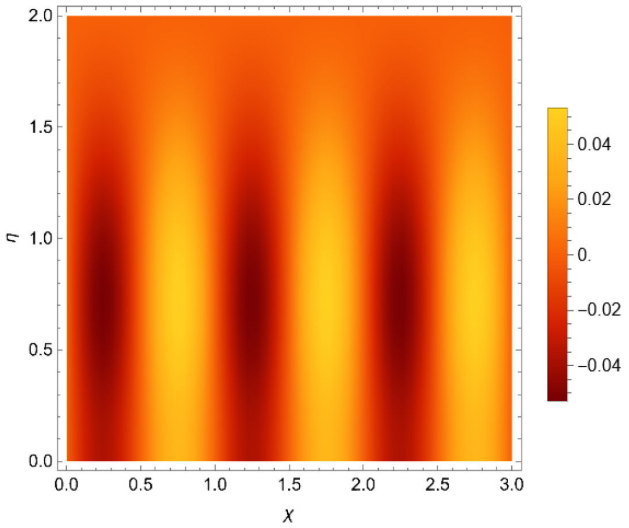

FIGURE 7. Spatial distribution of the transversal temperature gradient, $\partial\Theta/\partial\eta$, for $Pr = 5$, $De = 5$, $\varepsilon = 0.01$ and $a = 0.01$.

of the steady thermal component is not fully captured. It is therefore useful to examine the spatial distribution of the steady temperature gradient, $\partial\Theta_s/\partial\eta$, as shown in Fig. 7, where periodic elongated regions of positive and negative heat flux appear along the axial direction.

This makes the heat transfer over half of the wall wavelength especially relevant, since this interval defines the steady cooling and heating regions. The Nusselt number over the first half-wavelength ($\chi = 0$ to $\chi = 1/2$) for a complete temporal cycle is

$$\langle\overline{Nu}\rangle = \int_0^{2\pi}\left[\int_0^{1/2} -\left.\frac{\partial\Theta}{\partial\eta}\right|_{\eta=0} d\chi\right] d\tau = -2\pi a\lambda\left(\alpha^2+\beta(\beta-2\lambda)\right)/\left((2a+1)\left(\alpha^2+2\alpha\lambda+\beta^2-2\beta\lambda+2\lambda^2\right)\right), \quad (53)$$

while for the other half-wavelength is

$$\langle\overline{Nu}\rangle = \int_0^{2\pi}\left[\int_{1/2}^{1} -\left.\frac{\partial\Theta}{\partial\eta}\right|_{\eta=0} d\chi\right] d\tau = 2\pi a\lambda\left(\alpha^2+\beta(\beta-2\lambda)\right)/\left((2a+1)\left(\alpha^2+2\alpha\lambda+\beta^2-2\beta\lambda+2\lambda^2\right)\right). \quad (54)$$

Equations (53) and (54) characterize the stationary heat transfer zones along the wall.

4. Conclusions

We investigated the thermal behavior of a Maxwell viscoelastic fluid in the oscillatory boundary layer flow over a wavy wall. The waviness of the wall is introduced to model surface roughness, which plays a significant role at the microscale. Building on a previously derived velocity field-obtained via a perturbation method under the assumptions of small oscillation amplitude and a Stokes layer thickness much smaller than the wall wavelength [43]-we apply the same approach to solve the heat transfer equation, imposing a time-periodic temperature at the wall and a constant temperature at the boundary layer's outer edge.

At first order ($\mathcal{O}(\varepsilon^0)$) a purely diffusive temperature solution is found, corresponding to the thermal analogue of Stokes' second problem, with the temperature distribution exhibiting a phase shift relative to the wall temperature. At this order, the thermal problem is not influenced by the motion of the Maxwell fluid. Both the thermal penetration depth and the wavelength of the temperature distribution scale as $\delta/\sqrt{Pr}$, therefore, overdamped temperature oscillations result. Similarly to the fluid dynamic problem, the second-order ($\mathcal{O}(\varepsilon^1)$) temperature solution comprises a time-dependent distribution oscillating with twice the original frequency and a steady distribution, analogous to the steady streaming flow of the dynamical boundary layer problem. This behavior is promoted by the convective terms that involve the temperature field and velocity components at first order, and therefore, fluid viscoelasticity becomes relevant. Steady temperature fields resemble stream function patterns of the steady streaming flow [43], displaying alternated cold and hot elongated regions whose topology changes as the Deborah and Prandtl numbers vary.

Similarly to the fluid dynamics case, the steady temperature distribution approaches a finite value as the edge of the thermal boundary layer is reached, indicating the penetration of the steady temperature into the outer potential flow. In this context, a thermal generalization of Rayleigh's law of streaming was derived, which depends on the Deborah and Prandtl numbers. Specifically, for $De \gg 1$, the maximum temperature value penetrating the outer potential flow occurs when $Pr = (1/6)(1+2De)$, while in the Newtonian limit ($De = 0$), the maximum temperature value at the edge of the boundary layer ($\eta \to \infty$) is obtained when $Pr = 1+(2/\sqrt{3})$.

To characterize the outer thermal layer, where the steady temperature decays to zero, in analogy to the dynamic problem [13], a streaming Péclet number was introduced. When this parameter is small, a diffusion-dominated region forms; for large values, a secondary thermal boundary layer develops. The matching of the inner and outer steady temperature fields would require the use of the value given by the thermal Rayleigh's law of streaming as a boundary condition. Interestingly, the estimated thickness of the outer thermal boundary layer turned out to be independent of the fluid's viscoelasticity.

Given the growing interest in streaming flows at the microscale, exploring their heat transfer characteristics has become a worthwhile subject of study, particularly for applications such as heat transfer enhancement.

Appendix

A. Pressure distribution

Considering perturbation expansions on the small parameter ε, the pressure field can be expressed as

$$p(\chi,\tau) = p_0(\chi,\tau) + \varepsilon p_1(\chi,\tau) + \mathcal{O}(\varepsilon^2). \quad (A.1)$$

By substituting Eq. (A.1) in (19), the corresponding equations for the pressure field at different orders are obtained. At $\mathcal{O}(\varepsilon^0)$ the pressure satisfies

$$-\frac{\partial p_0}{\partial\chi} = 2\frac{\partial U}{\partial\tau}, \quad (A.2)$$

with the boundary condition $p_0(0,\tau) = G_0 e^{i\tau}$, where G_0 is a constant. Therefore, the first-order approximation for the pressure field is given by

$$p_0(\chi,\tau)=\left(G_0-\frac{2i\tanh^{-1}\left[\sqrt{-2a-1}\tan(\pi\chi)\right]}{\pi\sqrt{-2a-1}}\right)e^{i\tau}. \tag{A.3}$$

At $\mathcal{O}(\varepsilon^1)$ the pressure field satisfies

$$-\frac{\partial p_1}{\partial\chi}=2U\frac{\partial U}{\partial\chi}, \tag{A.4}$$

which is subject to the boundary condition $p_1(0,\tau)=0$. Similar to the velocity and temperature fields, the right-hand side of (A.4) contains convective terms that generate both unsteady contributions (at twice the oscillation frequency) and steady components. Hence, p_1 can be expressed as

$$p_1(\chi,\tau)=\Re\left\{p_{1u}(\chi)e^{2i\tau}+p_{1s}(\chi)\right\}. \tag{A.5}$$

The solution for the unsteady and steady components of the pressure field that satisfy the corresponding boundary conditions are given by

$$p_{1u}(\chi)=p_{1s}(\chi)=\frac{1}{2}-\frac{1}{2(a\cos(2\pi\chi)-a-1)^2}. \tag{A.6}$$

1. U. H. Kurzweg, Enhanced heat conduction in oscillating viscous flows within parallel-plate channels, *J. Fluid Mech.* **156** (1985) 291, https://doi.org/10.1017/S0022112085002105
2. A. Lambert *et al*., Heat transfer enhancement in oscillatory flows of Newtonian and viscoelastic fluids, *International Journal of Heat and Mass Transfer.* **52** (2009) 5472, https://doi.org/10.1016/j.ijheatmasstransfer.2009.07.001
3. P. C. Chatwin, On the longitudinal dispersion of passive contaminant in oscillatory flows in tubes, *J. Fluid Mech.* **71** (1975) 513, https://doi.org/10.1017/S0022112075002716
4. E. J. Watson, Diffusion in oscillatory pipe flow, *J. Fluid Mech.* **133** (1983) 233, https://doi.org/10.1017/S0022112083001883
5. J. C. Domínguez-Lozoya, H. Perales, and S. Cuevas, Analysis of the oscillatory liquid metal flow in an alternate MHD generator, *Rev. Mex. Fís.* **65** (2019) 239, https://doi.org/10.31349/revmexfis.65.239
6. C. Mei, Resonant reflection of surface water waves by periodic sandbars, *J. Fluid Mech.* **152** (1985) 315, https://doi.org/10.1017/S0022112085000714
7. P. Blondeaux, Sand ripples under sea waves Part 1. Ripple formation, *J. Fluid Mech.* **218** (1990) 1, https://doi.org/10.1017/S0022112090000908
8. H. Kumar, *et al*., Steady streaming: A key mixing mechanism in low-Reynolds-number acinar flows, *Phys. Fluids* **23** (2011) 041902, https://doi.org/10.1063/1.3567066
9. A. Sánchez, *et al*., On the bulk motion of the cerebrospinal fluid in the spinal canal, *J. Fluid Mech.* **841** (2018) 203, https://doi.org/10.1017/jfm.2018.67
10. G. G. Stokes, On the Effect of the Internal Friction of Fluids on the Motion of Pendulum, *Trans. Cambridge Phil. Soc.* **9** (1851) 8.
11. N. Riley, Steady Streaming, *Ann. Rev. Fluid Mech.* **33** (2001) 43, https://doi.org/10.1146/annurev.fluid.33.1.43
12. N. Riley, Unsteady laminar boundary layers, *SIAM Review* **17** (1975) 274.
13. J. T. Stuart, Double boundary layers in oscillatory viscous flows, *J. Fluid Mech.* **24** (1966) 673, https://doi.org/10.1017/S0022112066000910
14. L. Rayleigh, On the circulations of air observed in Kundt's tubes and or some allied acoustical problems, *Philosophical Transactions of the Royal Society A* **175** (1884) 1.
15. L. Rayleigh, The Theory of Sound, **vol. 2** (Dover, New York, 1945), pp. 333-342, Reprint of earlier work.
16. H. Schlichting, Berechnung ebner periodischer Grenzschichtstromungen, *Physikalische Zeitschrift* **33** (1932) 327.
17. H. Schlichting, Boundary Layer Theory, seventh ed. (McGraw-Hill, New York, 1979), pp. 428-432.
18. N. Riley, Oscillating viscous flow, *Mathematika* **12** (1965) 161, https://doi.org/10.1112/S0025579300005283
19. N. Riley, Oscillatory viscous flows: Review and extension, *IMA J. Appl. Math.* **3** (1967) 419, https://doi.org/10.1093/imamat/3.4.419
20. M. Wiklund, R. Green, and M. Ohlin, Acoustofluidics 14: Applications of acoustic streaming in microfluidic devices, *Lab Chip* **12** (2012) 2438, https://doi.org/10.1039/C2LC40203C
21. K. Sritharan *et al*., Acoustic mixing at low Reynolds numbers, *Appl. Phys. Lett.* **88** (2006) 054102, https://doi.org/10.1063/1.2171482
22. D. Ahmed *et al*., A millisecond micromixer via single-bubblebased acoustic streaming, *Lab Chip* **9** (2009) 2738, https://doi.org/10.1039/B903687C
23. X. Zhang, J. Minten, and B. Rallabandi, Particle hydrodynamics in acoustic fields: Unifying acoustophoresis with streaming, *Phys. Rev. Fluids* **9** (2024) 044303, https://doi.org/10.1103/PhysRevFluids.9.044303
24. B. Lutz, J. Chen, and D. T. Schwartz, Hydrodynamic tweezers: 1. Noncontact trapping of single cells using steady streaming microeddies, *Anal. Chem.* **78** (2006) 5429, https://doi.org/10.1021/ac060555y
25. R. Thameem, B. Rallabandi, and S. Hilgenfeldt, Fast inertial particle manipulation in oscillating flows, *Phys. Rev. Fluids* **2** (2017) 052001(R), https://doi.org/10.1103/PhysRevFluids.2.052001

26. Y. Bhosale, T. Parthasarathy, and M. Gazzola, Soft streaming - flow rectification via elastic boundaries, *J. Fluid Mech.* **945** (2022) R1, https://doi.org/10.1017/jfm.2022.525

27. C. F. Chang, Boundary layer analysis of oscillating cylinder flows in a viscoelastic liquid, *J. Appl. Math. Phys. (ZAMP)* **28** (1977) 283, https://doi.org/10.1007/BF01595595

28. C.-F. Chang and W. Schowalter, Secondary flow in the neighborhood of a cylinder oscillating in a viscoelastic fluid, *J. Non-Newton. Fluid Mech.* **6** (1979) 47, https://doi.org/10.1016/0377-0257(79)87003-2

29. K. R. Frater, Secondary flow in an elastico-viscous fluid caused by rotational oscillations of a sphere. Part 1, *J. Fluid Mech.* **20** (1964) 369, https://doi.org/10.1017/S0022112064001288

30. G. Böhme, On steady streaming in viscoelastic liquids, J. Non-Newton. *Fluid Mech.* **44** (1992) 149, https://doi.org/10.1016/0377-0257(92)80049-4

31. P. D. Richardson, Heat transfer from a circular cylinder by acoustic streaming, *J. Fluid Mech.* **30** (1967) 337, https://doi.org/10.1017/S0022112067001466

32. B. J. Davidson, Heat transfer from a vibrating circular cylinder, *Int. J. Heat Mass Transfer* **16** (1973) 1703, https://doi.org/10.1016/0017-9310(73)90163-4

33. A. Gopinath and A. F. Mills, Convective heat transfer from a sphere due to acoustic streaming, *ASME J. Heat Transfer* **115** (1993) 332, https://doi.org/10.1115/1.2910684

34. A. Gopinath and A. F. Mills, Convective heat transfer due to acoustic streaming across the ends of a Kundt tube, *ASME J. Heat Transfer* **116** (1994) 47, https://doi.org/10.1115/1.2910882

35. S. Cuevas and E. Ramos, Transport of Momentum and Heat in Oscillatory MHD Flow, In A. Alemany, P. Marty, and J. P. Thibault, eds., Transfer Phenomena in Magnetohydrodynamic and Electroconducting Flows: Selected papers of the PAMIR Conference held in Aussois, France 22-26 September 1997, pp. 107-122 (Springer Netherlands, Dordrecht, 1999), https://doi.org/10.1007/978-94-011-4764-4_8.

36. A. Gopinath and D. R. Harder, An experimental study of heat transfer from a cylinder in low-amplitude zero-mean oscillatory flows, *Int. J. Heat Mass Transfer* **43** (2000) 505, https://doi.org/10.1016/S0017-9310(99)00138-6

37. A. Gopinath, Thermoacoustic streaming on a sphere, *Proc. R. Soc. Lond. A* **456** (2000) 2419, https://doi.org/10.1098/rspa.2000.0619

38. S. Hyun, D.-R. Lee, and B.-G. Loh, Investigation of convective heat transfer augmentation using acoustic streaming generated by ultrasonic vibrations, *Int. J. Heat Mass Transfer* **48** (2005) 703, https://doi.org/10.1016/j.ijheatmasstransfer.2004.07.048

39. M. Rahimi, M. Dehbani, and M. Abolhasani, Experimental study on the effects of acoustic streaming of high frequency ultrasonic waves on convective heat transfer: Effects of transducer position and wave interference, *Int. Comm. Heat Mass Transfer* **39** (2012) 720, https://doi.org/10.1016/j.icheatmasstransfer.2012.03.013

40. Y. Liu *et al*., Numerical simulation on acoustic streaming characteristics in boiler tube array, *In. J. Heat Mass Transfer* **193** (2022) 122834, https://doi.org/10.1016/j.ijheatmasstransfer.2022.122834

41. D. Zhan, *et al*., Investigation on the heat transfer performance of microchannel with combined ultrasonic and passive structure, *Appl. Thermal Eng.* **233** (2023) 121076, https://doi.org/10.1016/j.applthermaleng.2023.121076

42. D. Zhang *et al*., Investigation of flow and heat transfer characteristics in microchannel with high-frequency ultrasound, Thermal *Sci. Eng. Prog* **59** (2025) 103305, https://doi.org/10.1016/j.tsep.2025.103305

43. S. Cuevas, J. C. Domínguez-Lozoya, and L. Córdova- Castillo, Oscillatory boundary layer flow of a Maxwell fluid over a wavy wall, *J. Non-Newton. Fluid Mech.* **321** (2023) 105125, https://doi.org/10.1016/j.jnnfm.2023.105125

44. C.-C. Cho, C.-L. Chen, and C. Chen, Electrokineticallydriven non-Newtonian fluid flow in rough microchannel with complex-wavy surface, *J. Non-Newton. Fluid Mech.* **173-174** (2012) 13, https://doi.org/10.1016/j.jnnfm.2012.01.012

45. L. Martínez *et al*., Electroosmotic flow of a Phan- Thien-Tanner fluid in a wavy-wall microchannel, *Colloids and Surfaces A: Physicochem. Eng. Aspects* **498** (2016) 7, https://doi.org/10.1016/j.colsurfa.2016.02.036

46. J. Arcos *et al*., Analysis of an electroosmotic flow in wavy wall microchannels using the lubrication approximation, *Rev. Mex. Fís.* **66** (2020) 761, https://doi.org/10.31349/RevMexFis.66.761

47. M. López de Haro, J. A. del Río, and S. Whitaker, Flow of Maxwell fluids in porous media, *Transp. Porous Media* **25** (1996) 167, https://doi.org/10.1007/BF00135854

48. F. A. Morrison, Understanding rheology (Oxford University Press, 2001).